Physics Letters B 737 (2014) 75–80

Contents lists available at ScienceDirect

Physics Letters B

www.elsevier.com/locate/physletb

Resonance dynamics in the coherent η meson production in the (p, p') reaction on the spin–isospin saturated nucleus

Swapan Das

Nuclear Physics Division, Bhabha Atomic Research Centre, Mumbai 400085, India

ARTICLE INFO

Article history:
Received 12 May 2014
Received in revised form 1 August 2014
Accepted 8 August 2014
Available online 13 August 2014
Editor: W. Haxton

Keywords:
η meson exchange interaction
N^* propagation

ABSTRACT

For the forward going proton and η meson, the coherent η meson production in the (p, p') reaction on the spin–isospin saturated nucleus occurs only due to the η meson exchange interaction between the beam proton and nucleus. In this process, the nucleon in the nucleus can be excited to resonances N^* and the η meson in the final state can arise due to $N^* \to N\eta$. We investigate the dynamics of resonances, including nucleon Born terms, and their interferences in the coherently added cross section of this reaction. We discuss the importance of $N(1520)$ resonance and show the sensitivity of the cross section to the hadron–nucleus interaction.

The coherent meson production in the nuclear reaction is a potential tool to investigate the resonance dynamics in the nucleus, as well as the meson–nucleus interaction in the final state. Since the branching ratio of $\Delta(1232) \to N\pi$ is $\simeq$ 100% [1], the coherent pion production process has been used extensively to investigate the Δ dynamics in the nucleus [2,3]. This process in (γ, π) and $(e, e\pi)$ reactions is used to study the transverse $N \to \Delta$ excitation in the nucleus, where the coherent pion is produced away from the forward direction [4]. The forward emission of coherent pion is a probe for the longitudinal Δ excitation which occur in the pion nuclear reaction [5].

The coherent pion production is also studied in the proton and ion induced nuclear reaction [6,7]. The issue of Δ-peak shift in the nucleus [8] is resolved, as it occurs because of the coherent pion production [6,7] which is not possible for proton target. The coherent pion production in the (p, n) [6] and $(^3\mathrm{He}, t)$ [7] reactions on the nucleus is shown to have one to one correspondence with that in the π^+ meson–nucleus scattering [9,10]. For the forward going protons, the coherent pion production in the (p, p') reaction can be used to produce π^0 beam [11] which is analogous to tagged photon beam.

The coherent η meson production in the nuclear reaction is another process which can be used to study the resonance dynamics in the nucleus. Amongst the resonances, $N(1535)$ has large decay branching ratio (42%) in the $N\eta$ channel, i.e., $\Gamma_{N(1535)\to N\eta}(m = 1535\ \mathrm{MeV}) \approx 63$ MeV [1]. Therefore, this resonance is considered to study the coherent η meson production in the proton–nucleus reaction [12]. $N(1535)$ is shown as a sensitive probe to study the non-local effects in the coherent η meson photoproduction reaction [13]. The importance of $N(1535)$ is elucidated in context of the η meson production in the hadron–nucleus reaction [14]. In addition to $N(1535)$, other resonances, e.g., $N(1520)$, $N(1650)$ etc., (whose branching ratio in the $N\eta$ channel is much less than that of $N(1535)$) and nucleon Born terms are also considered in the study of η meson production in the photonuclear reaction below 1 GeV [15]. The change in the cross section because of the interference of $N(1520)$ and $N(1535)$ resonances is described in Ref. [16].

Sometime back, Alvaredo and Oset studied the coherent η meson production in the (p, p') reaction on the spin–isospin saturated nucleus [12]: $p + A(gs) \to p' + A(gs) + \eta$. The elementary reaction in the nucleus is assumed to proceed as $pN \to p'N^*$; $N^* \to N\eta$ (presented in Fig. 1). The resonance N^* considered in the intermediate state is $N(1535)$, since it has large branching ratio (as mentioned earlier) in the $N\eta$ channel. This resonance is produced due to the η meson (a pseudoscalar–isoscalar meson) exchange interaction only, specifically, for the forward going proton and η meson. The contributions from other meson exchange interactions vanish in this reaction [12]. The projectile excitation in this reaction is null for the spin saturated nucleus.

It may be argued that though the resonance $N(1520)$ has very small decay width (at its pole mass) in the $N\eta$ channel, there are enough reasons (mentioned below) not to neglect this resonance in the η meson production reaction.

(i) The mass of $N(1520)$ is close to that of $N(1535)$, and therefore there could be interference effect in the η meson production reaction [16], as quoted above.

E-mail address: swapand@barc.gov.in.

http://dx.doi.org/10.1016/j.physletb.2014.08.019

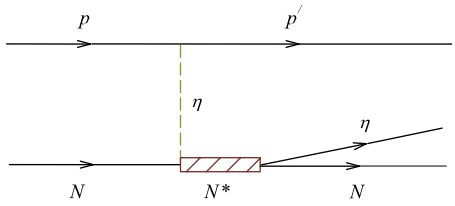

Fig. 1. (Color online.) Elementary reaction occurring in the nucleus.

Table 1
Blatt–Weisskopf barrier-penetration factor $B_l(\tilde{k}R)$ [18].

N^*	l	$B_l^2(x=\tilde{k}R)$
$N(1520)$	2	$x^4/(9+3x^2+x^4)$
$N(1535)$	0	1

(ii) The earlier value for $\Gamma_{N(1520)\to N\eta}(m=1520\ \text{MeV})$, as reported in Ref. [17], is 0.12 MeV, which corresponds to the coupling constant: $f_{\eta NN(1520)}=6.72$ [13]. According to the recent result: $\Gamma_{N(1520)\to N\eta}(m=1520\ \text{MeV})\simeq 0.265$ MeV [1], the value of $f_{\eta NN(1520)}$ is equal to 9.98. The latter value of $f_{\eta NN(1520)}$ is about 1.5 times larger than its previous value. Due to this enhancement, the coherent η meson production cross section because of $N(1520)$ is increased by a factor about 5.

(iii) The decay width $\Gamma_{N^*\to N\eta}(m)$ varies with the mass m of the resonance N^* [18] as

$$\Gamma_{N^*\to N\eta}(m)=\Gamma_{N^*\to N\eta}(m_{N^*})\left[\frac{\Phi_l(m)}{\Phi_l(m_{N^*})}\right]. \tag{1}$$

m_{N^*} in this equation is the pole mass of N^*. The value of $\Gamma_{N^*\to N\eta}(m_{N^*})$ is already mentioned for $N(1520)$ and $N(1535)$ resonances. The suffix l in the phase-space factor Φ_l represents the angular momentum associated with the decay. Φ_l is given by $\Phi_l(m)=\frac{\tilde{k}}{m}B_l^2(\tilde{k}R)$, where $\tilde{k}$ is the relative momentum of the decay products (i.e., N and η) in their c.m. frame. $B_l(\tilde{k}R)$ is the Blatt–Weisskopf barrier-penetration factor, listed in Table 1. R (= 0.25 fm) is the interaction radius. Using Eq. (1), we show in Fig. 2 that the decay probability of $N(1520)\to N\eta$ rises sharply over that of $N(1535)\to N\eta$ with the increase in resonance mass m, i.e., ηN invariant mass. Therefore, though the decay width of $N(1520)\to N\eta$ at the pole mass, as quoted earlier, is much less than that of $N(1535)\to N\eta$, the previous (as shown in Fig. 2) supersedes the latter at higher values of m. The steep rise in $\Gamma_{N(1520)\to N\eta}(m)$ with m can shift the peak position of the η meson production cross section due to $N(1520)$ towards the larger value of m.

We have elucidated that the cross section due to $N(1520)$ in the η meson production reaction could be large. This can change the shape and magnitude of the coherently added cross section arising due to nucleon Born terms and resonances. To disentangle it, we revisit the coherent η meson production in the (p,p') reaction on the scalar–isoscalar nucleus where Born terms, $N(1520)$ and other resonances of $N\eta$ branching ratio $\geq 4\%$, i.e., $N(1535)$, $N(1650)$, $N(1710)$, $N(1720)$, are considered. In this reaction, the virtual η meson (emitted by projectile) is elastically scattered to its real state by the nucleus which remains in its ground state. Since ^{4}He does not have excited state, this nucleus is preferred to study the mechanism of this reaction. In the experiment both coherent production and breakup will occur, but the coherent channel can in principle be identified.

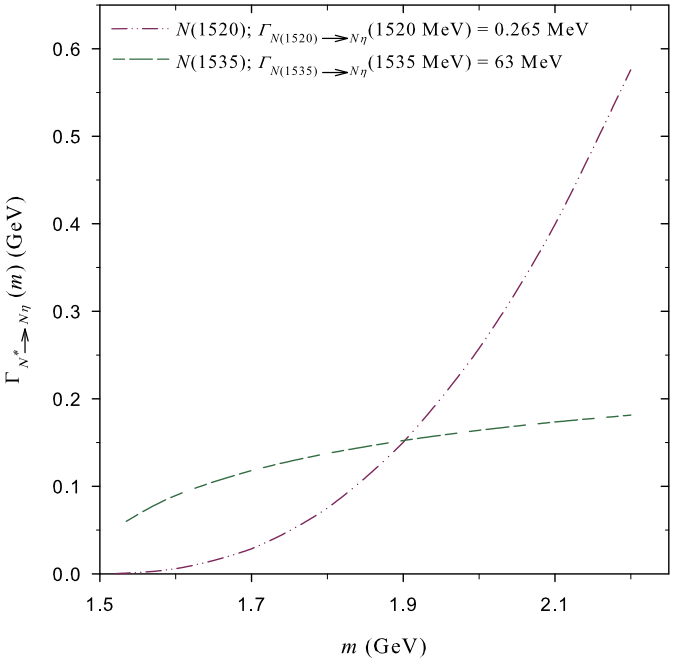

Fig. 2. (Color online.) Decay width $\Gamma_{N^*\to N\eta}(m)$ vs. resonance mass m.

The Lagrangian $\mathcal{L}$ for the coupling of η meson to a particle depends on their spin and parity [13,16]. For $\frac{1}{2}^+$ particle, i.e., $N(940)$ and $N^*\equiv N(1710)$, the form for $\mathcal{L}$ is

$$\begin{aligned}\mathcal{L}_{\eta NN}&=-ig_\eta F_\eta(q^2)\bar{N}\gamma_5 N\eta\\ \mathcal{L}_{\eta NN^*}&=-ig_\eta^* F_\eta^*(q^2)\bar{N}^*\gamma_5 N\eta;\end{aligned} \tag{2}$$

g_η (ηNN coupling constant) $\simeq 7.93$ [20], and g_η^* ($\eta NN(1710)$ coupling constant) $\simeq 4.26$. For $\frac{1}{2}^-$ resonance N^*, i.e., $N(1535)$ and $N(1650)$, $\mathcal{L}$ is given by

$$\mathcal{L}_{\eta NN^*}=-ig_\eta^* F_\eta^*(q^2)\bar{N}^* N\eta; \tag{3}$$

$g_\eta^*\simeq 1.86$ for $N(1535)$ and $g_\eta^*\simeq 0.67$ for $N(1650)$. For $N(1520)\frac{3}{2}^-$, $\mathcal{L}$ can be written as

$$\mathcal{L}_{\eta NN^*}=\frac{f_\eta^*}{m_\eta}F_\eta^*(q^2)\bar{N}^{*\mu}\gamma_5 N\partial_\mu\eta; \tag{4}$$

$f_\eta^*=9.98$. For $\frac{3}{2}^+$ resonance [19], i.e., $N^*\equiv N(1720)$, the expression for $\mathcal{L}$ is

$$\mathcal{L}_{\eta NN^*}=\frac{f_\eta^*}{m_\eta}F_\eta^*(q^2)\bar{N}^{*\mu}N\partial_\mu\eta; \tag{5}$$

$f_\eta^*=1.15$. The coupling constants are extracted from the measured decay width of the resonances, i.e., $N^*\to N\eta$ [1]. F_η and F_η^* appearing in Lagrangians are the ηNN and ηNN^* form factors respectively [20]: $F_\eta(q^2)=F_\eta^*(q^2)=\frac{\Lambda_\eta^2-m_\eta^2}{\Lambda_\eta^2-q^2}$; $\Lambda_\eta=1.5$ GeV.

The T-matrix for the coherent η meson production in the (p,p') reaction on a nucleus can be written as $T_{fi}=T_B+T_{N^*}$, where T_B represents the T-matrix for nucleon Born terms (described later), and the resonance term, i.e., T_{N^*}, is given by

$$\begin{aligned}T_{N^*}=\sum_{N^*}\hat{\Gamma}_{N^*\to N\eta}A(S)\tilde{V}_\eta(q)\int d\mathbf{r}\chi^{(-)*}(\mathbf{k}_\eta,\mathbf{r})G_{N^*}(m,\mathbf{r})\\ \times\varrho(\mathbf{r})\chi^{(-)*}(\mathbf{k}_{p'},\mathbf{r})\chi^{(+)}(\mathbf{k}_p,\mathbf{r}).\end{aligned} \tag{6}$$

Table 2
$\Lambda(S)$ for spin $S = \frac{1}{2}$ and $\frac{3}{2}$ fermions.

Spin (S)	$\Lambda(S)$
$\frac{1}{2}$	$\{\not{k} + m_{N^*}\}$
$\frac{3}{2}$	$\{\not{k} + m_{N^*}\}\left[g^{\mu}_{\nu} - \frac{\gamma^{\mu}\gamma_{\nu}}{3} - \frac{\gamma^{\mu}k_{\nu} - \gamma^{\nu}k_{\mu}}{3m_{N^*}} - \frac{2k^{\mu}k_{\nu}}{3m^2_{N^*}}\right]$

$\varrho(\mathbf{r})$ in this equation is the matter density distribution of the nucleus. $\hat{\Gamma}_{N^*\to N\eta}$ denotes the vertex factor for the decay: $N^* \to N\eta$. The spin S dependent part of N^* propagator, i.e., $\Lambda(S)$, is expressed in Table 2.

$\tilde{V}_{\eta}(q)$ in above equation represents the η meson exchange interaction between the beam proton and the nucleon in the nucleus (see Fig. 1): $\tilde{V}_{\eta}(q) = \hat{\Gamma}_{\eta NN^*}\tilde{G}_{\eta}(q^2)\hat{\Gamma}_{\eta NN}$. The $\hat{\Gamma}$s are described by the Lagrangians given in Eqs. (2)–(5). $\tilde{G}_{\eta}(q^2)$ denotes the virtual η meson propagator, given by $\tilde{G}_{\eta}(q^2) = -\frac{1}{m^2_{\eta}-q^2}$.

The distorted wave functions for proton and η meson, denoted by χs in Eq. (6), are evaluated by using the Glauber model [21]. For the beam proton p, it can be written as

$$\chi^{(+)}(\mathbf{k}_p, \mathbf{r}) = e^{i\mathbf{k}_p\cdot\mathbf{r}}\exp\left[-\frac{i}{v_p}\int_{-\infty}^{z} dz' V_{Op}(\mathbf{b}, z')\right]. \tag{7}$$

For outgoing particles, i.e., p' and η meson, χ is given by

$$\chi^{(-)^*}(\mathbf{k}_{p'(\eta)}, \mathbf{r}) = e^{-i\mathbf{k}_{p'(\eta)}\cdot\mathbf{r}}\exp\left[-\frac{i}{v_{p'(\eta)}}\int_{z}^{+\infty} dz' V_{Op'(\eta)}(\mathbf{b}, z')\right]. \tag{8}$$

v_X is the velocity of the particle X which is either proton or η meson appearing in Eqs. (7) and (8). V_{OX} denotes the particle–nucleus optical potential. This potential, in fact, describes the initial and final state interactions.

The proton–nucleus optical potential $V_{Op(p')}(\mathbf{r})$ in Eqs. (7) and (8) is calculated using the "$t\varrho(\mathbf{r})$" approximation [21], i.e.,

$$V_{Op}(\mathbf{r}) = -\frac{v_p}{2}[i + \alpha_{pN}]\sigma_t^{pN}\varrho(\mathbf{r}), \tag{9}$$

where α_{pN} denotes the ratio of the real to imaginary part of the proton–nucleon scattering amplitude f_{pN}. σ_t^{pN} represents the corresponding total cross section. To evaluate this potential, we use the energy dependent experimentally determined values for α_{pN} and σ_t^{pN} [22].

The η meson–nucleus optical potential $V_{O\eta}(\mathbf{r})$ in Eq. (8), following Alvaredo and Oset [12], is evaluated from the η meson self-energy $\Pi_{\eta}(\mathbf{r})$ in the nucleus:

$$\Pi_{\eta}(\mathbf{r}) = 2E_{\eta}V_{O\eta}(\mathbf{r}) = \sum_{N^*}\left|C(N^*)\right|^2\frac{\varrho(\mathbf{r})}{m - m_{N^*} + \frac{i}{2}\Gamma_{N^*}(m) - V_{ON^*}(\mathbf{r}) + V_{ON}(\mathbf{r})}. \tag{10}$$

The prefactor $C(N^*)$ depends on the resonance N^* used to calculate $\Pi_{\eta}(\mathbf{r})$. $\Gamma_{N^*}(m)$ represents the total width of N^* for its mass equal to m. It is composed of partial widths of N^* decaying into various channels, listed duly along with the physical parameters in Ref. [1]. The resonance mass m dependence of these widths are worked out following Eq. (1). Values of $\Gamma_{N^*}(m)$ at the pole mass, i.e., $m = m_{N^*}$, are given in Table 3. V_{ON^*} is the N^* nucleus interacting potential, described latter. The nucleon potential energy in the nucleus is taken as $V_{ON}(\mathbf{r}) = -50\varrho(\mathbf{r})/\varrho(0)$ MeV [12]. $\Pi_{\eta}(\mathbf{r})$ arising due to nucleon–hole pair is evaluated following that for π^0 meson, see page 157 in Ref. [3].

Table 3
Resonance width $\Gamma_{N^*}(m_{N^*})$ at pole mass m_{N^*} in MeV [1].

Resonance N^*	$\Gamma_{N^*}(m_{N^*})$
$N(1520)$	115
$N(1535)$	150
$N(1650)$	150
$N(1710)$	100
$N(1720)$	250

The scalar part of the resonance propagator, denoted by $G_{N^*}(m, \mathbf{r})$ in Eq. (6), is given by

$$G_{N^*}(m, \mathbf{r}) = \frac{1}{m^2 - m^2_{N^*} + im_{N^*}\Gamma_{N^*}(m) - 2E_{N^*}V_{ON^*}(\mathbf{r})}, \tag{11}$$

where E_{N^*} denotes the energy of N^*.

$V_{ON^*}(\mathbf{r})$ in Eqs. (10) and (11), which describes the N^*–nucleus interaction, is also evaluated by using the "$t\varrho(\mathbf{r})$" approximation, as given in Eq. (9). In this case, the measured values of the N^*–nucleon scattering parameters, i.e., α_{N^*N} and $\sigma_t^{N^*N}$, are not available. To estimate them, we take $\alpha_{N^*N} \simeq \alpha_{NN}$ and $\sigma_{el}^{N^*N} \simeq \sigma_{el}^{NN}$ since the elastic scattering dynamics of N^* can be assumed not much different from that of a nucleon. For the reactive part of $\sigma_t^{N^*N}$, we consider that the dynamics of N^* is the same as that of a nucleon at its kinetic energy enhanced by Δm, i.e., $\sigma_r^{N^*N}(T_{N^*N}) \approx \sigma_r^{NN}(T_{N^*N} + \Delta m)$ [23]. Here, Δm is the mass difference between the resonance and nucleon. T_{N^*N} is the total kinetic energy in the N^*N center of mass system [23].

The η meson emitted because of the nucleon Born terms is addressed by T_B above Eq. (6). It is similar to the expression appearing in this equation except the interaction vertices and propagator of N^* to be replaced by those of nucleon. The previous is described by $\mathcal{L}_{\eta NN}$ in Eq. (2) and the latter, i.e., propagators G_N, are discussed in Ref. [2]. However, the calculated cross section due to Born terms, as shown later, is negligibly small.

We calculate the differential cross section, i.e., $\frac{d\sigma}{dE_{p'}d\Omega_{p'}d\Omega_{\eta}}$, for the forward going coherent η meson energy E_{η} distribution in the (p, p') reaction on ^{4}He nucleus. The calculated results are presented in Figs. 3 and 4. On the upper x-axis of these figures, we mention the resonance mass m corresponding to E_{η}. The spatial density distribution $\varrho(\mathbf{r})$ of this nucleus is $\varrho(\mathbf{r}) = \varrho_0\frac{1+w(r/c)^2}{1+e^{(r-c)/z}}$; $w = 0.445$, $c = 1.008$ fm, $z = 0.327$ fm [24]. We discuss the contribution of each resonance and nucleon Born terms (including their interferences) to the cross section of this reaction. We focus on two aspects of $N(1520)$ which can change the η meson production cross section considerably: (i) measured decay width $\Gamma_{N(1520)\to N\eta}(m = 1520$ MeV) and (ii) decay probability $N(1520) \to N\eta$ specifically at high energy.

The calculated plane wave results at $T_p = 1.2$ GeV are illustrated in Fig. 3(a), where the N^*–nucleus interaction is not included, i.e., $V_{ON^*} = (0, 0)$. The cross sections arising due to each resonance and Born terms along with their coherent contribution are shown in this figure. For $N(1520)$ resonance, the measured value of its decay width $\Gamma_{N(1520)\to N\eta}(m = 1520$ MeV) is taken equal to 0.12 MeV (earlier value). This figure elucidates that the cross section due to $N(1535)$, shown by short–long–short dash curve, is the largest. The dot–dot–dash curve represents the second largest cross section (which is 24.7% of the previous at the peak) arising because of $N(1520)$. The peak cross section due to it appears at higher value of E_{η} (which corresponds to larger m) compared to that because of $N(1535)$. This occurs, as described in Fig. 2, due to the sharp rise in $N(1520) \to N\eta$ decay probability

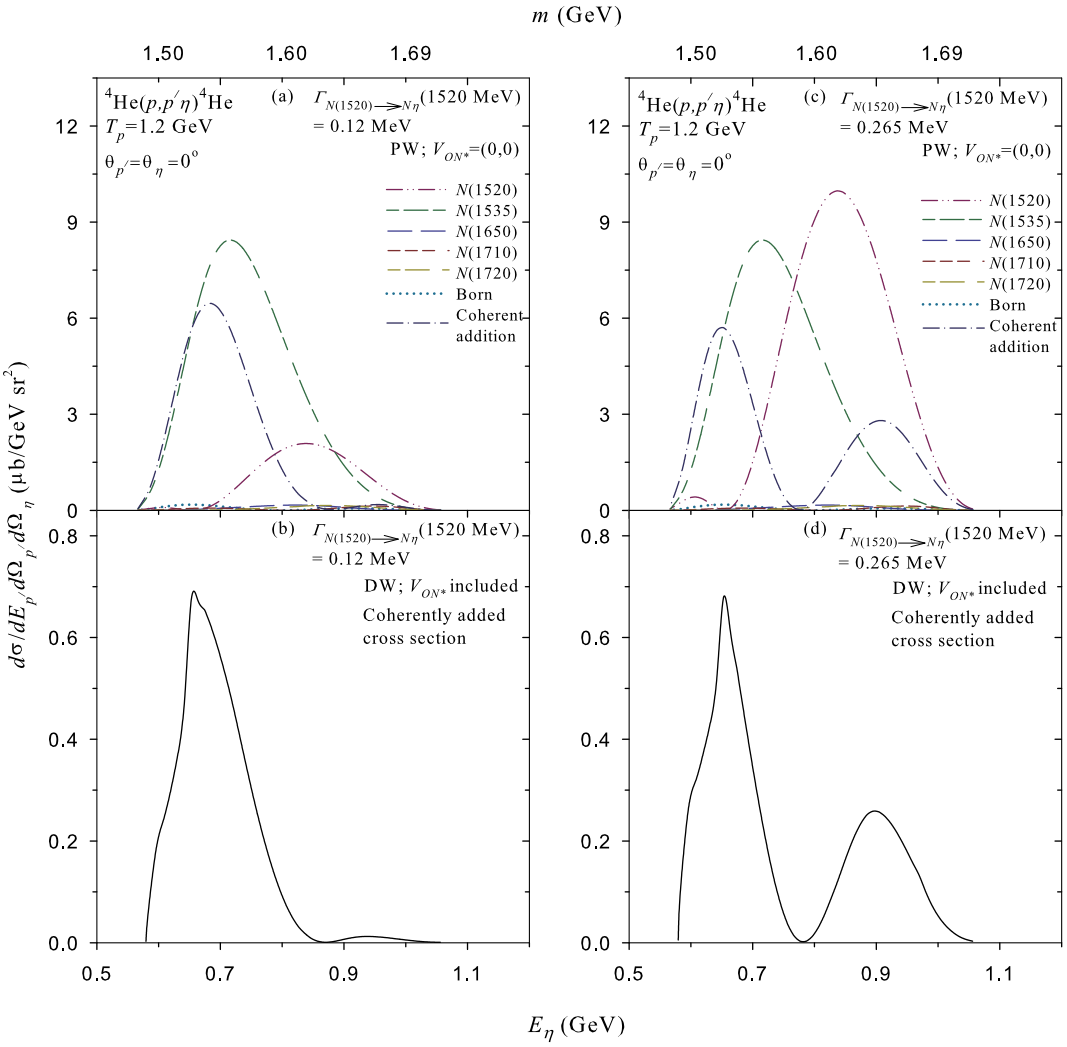

Fig. 3. (Color online.) Cross sections for the coherent η meson production at $T_p = 1.2$ GeV. m is the resonance mass corresponding to the η meson energy E_η (see text).

with m. Fig. 3(a) also shows that the cross sections arising because of other resonances and Born terms are negligibly small. The coherently added cross section (dot–dash curve) shows that the dominant contribution to it arises due to $N(1535)$. The effect of interference in the cross section is distinctly visible in this figure. In Fig. 3(b), we present the distorted wave results where V_{ON^*} is also incorporated. It shows that the cross section is reduced drastically, i.e., by a factor of 9.6 at the peak, and the peak position is shifted by 32 MeV towards the lower value of E_η due to the inclusion of distortions (both initial and final states) and V_{ON^*}. These are the features usually reported in the low energy η meson production reaction.

As stated earlier, the calculated cross section due to $N(1520)$ can go up by a factor of ∼5 because of the use of the latest measured value of $\Gamma_{N(1520)\to N\eta}(m = 1520$ MeV), i.e., 0.265 MeV. This can change the η meson energy E_η distribution of the coherently added cross section. We illustrate those in Fig. 3(c). It is remarkable that the cross section due to $N(1520)$ for $\Gamma_{N(1520)\to N\eta}(m = 1520$ MeV) $= 0.265$ MeV (dot–dot–dash curve) is comparable with that because of $N(1535)$ (short–long–short dash curve). In fact, the previous is about 18% larger than the latter. Due to this, an additional peak in the spectrum of the coherently added cross section (dot–dash curve) appears close to the peak arising because of $N(1520)$. The magnitude of the cross section due to the inclusion of distortions and V_{ON^*}, as shown in Fig. 3(d), is reduced drastically, but the change in the shape of spectrum due to them is insignificant. Two peaks are distinctly visible in this figure.

The decay probability of $N(1520) \to N\eta$, as shown in Fig. 2, rises sharply at higher values of the resonance mass m. Therefore, this resonance could be more significant in the high energy η meson production reaction. To investigate it, we calculate the plane wave (without V_{ON^*} included) cross sections at $T_p =$ 2.5 GeV (taking the earlier value of $\Gamma_{N(1520)\to N\eta}(m = 1520$ MeV), i.e., 0.12 MeV), and present those in Fig. 4(a). The cross sections arising because of each resonance and Born terms along with the coherently added cross section are distinctly visible in this figure. Compared to the spectra presented in Fig. 3(a), there are considerable changes in those at $T_p = 2.5$ GeV which are noticeable in Fig. 4(a). Three distinct peaks in the latter figure arise due to $N(1520)$ (dot–dot–dash curve), $N(1535)$ (short–long–short dash curve) and $N(1710)$ (short dash curve). Amongst them, the cross section because of $N(1520)$ is the largest. The cross sections due to resonances other than these three resonances and Born terms are insignificant. The separation between the peaks of the cross sections due to $N(1520)$ and $N(1535)$ at $T_p = 2.5$ GeV is larger than that found at $T_p = 1.2$ GeV (see Figs. 3(a) and 4(a)). This occurs, as illustrated in Fig. 2, because of the sharp increase in $N(1520) \to N\eta$ decay probability with m.

Because of the large η meson production cross section due to $N(1520)$ at $T_p = 2.5$ GeV (even for $\Gamma_{N(1520)\to N\eta}(m = 1520$ MeV) =

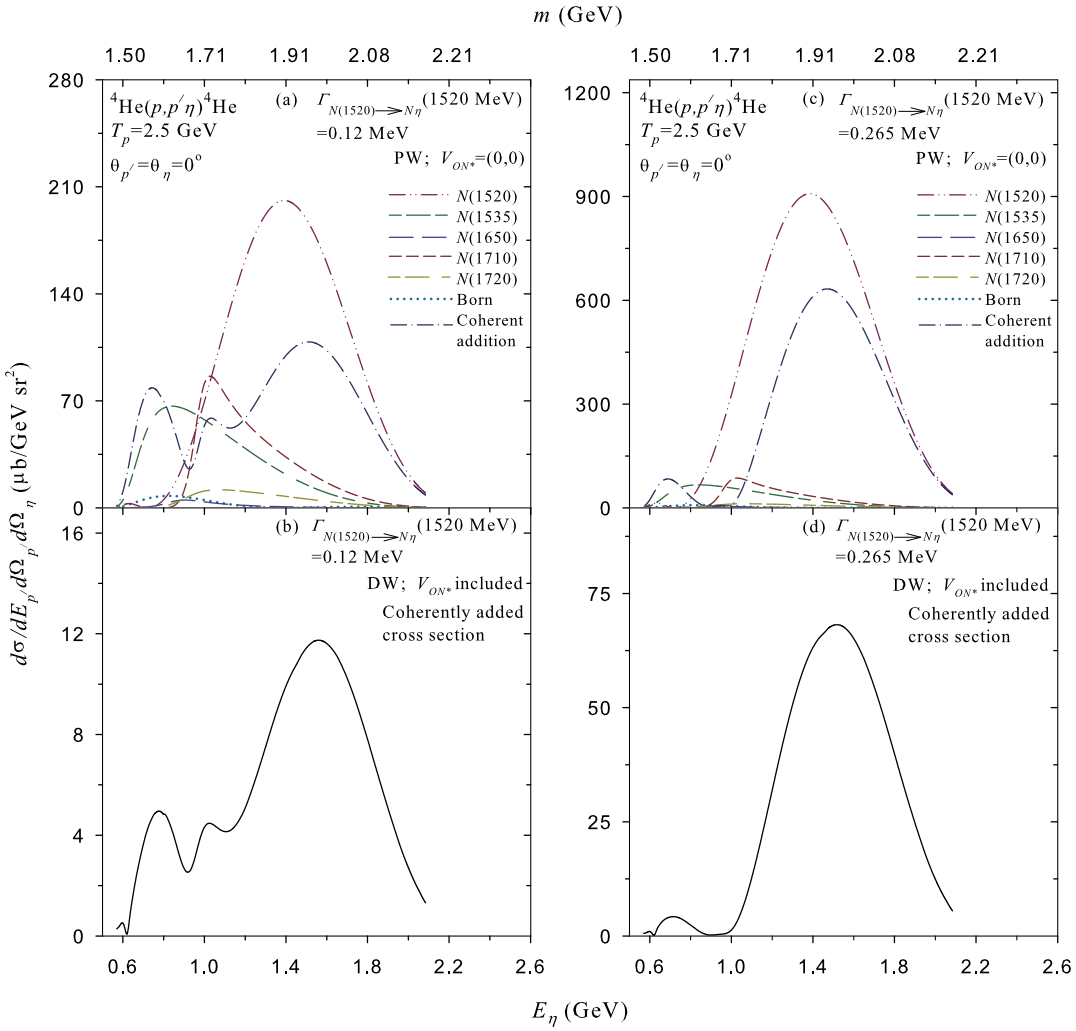

Fig. 4. (Color online.) Same as Fig. 3 but for the beam energy $T_p = 2.5$ GeV (see text).

0.12 MeV), the shape of the η meson energy E_η distribution spectrum of the coherently added cross section is significantly different from that calculated at $T_p = 1.2$ GeV (see dot–dash curves in Fig. 3(a) and Fig. 4(a)). We show the distorted wave (V_{ON^*} included) result at $T_p = 2.5$ GeV in Fig. 4(b). Both Figs. 4(a) and 4(b) show that the coherently added cross sections possess multiple peaks appearing in the peak regions of the cross sections due to $N(1520)$, $N(1535)$ and $N(1710)$ resonances. In addition, these figures elucidate that the largest peak arises in the $N(1520)$ excitation region. These results are unlike to those presented in Figs. 3(a) and 3(b).

The calculated plane wave, without V_{ON^*} included, cross section at $T_p = 2.5$ GeV due to $N(1520)$ for the latest value of $\Gamma_{N(1520)\to N\eta}(m = 1520$ MeV), i.e., 0.265 MeV, is presented by the dot–dot–dash curve in Fig. 4(c). Along with it, the cross sections because of other resonances and Born terms are also presented for comparison. Due to the increase in $\Gamma_{N(1520)\to N\eta}(m = 1520$ MeV), in addition to large $N(1520) \to N\eta$ decay probability at higher energy, the η meson production (as shown in this figure) dominantly occurs because of the $N(1520)$ resonance. In fact, the peak cross section due to it is distinctly the largest. The coherently added cross section (dot–dash curve in Fig. 4(c)) shows a small peak close to that because of $N(1535)$ and a large peak distinctly visible near to that due to $N(1520)$. We illustrate the distorted wave (V_{ON^*} included) result for it in Fig. 4(d). The dominant contribution to the coherently added cross section, as shown in Figs. 4(c) and 4(d), distinctly arises because of the resonance $N(1520)$.

We have calculated the differential cross sections for the coherent η meson energy E_η distribution in the (p, p') reaction on ^{4}He nucleus. At lower beam energy, i.e., 1.2 GeV, the cross section because of $N(1535)$ is distinctly the largest if we consider the earlier value of the decay width $\Gamma_{N(1520)\to N\eta}(m = 1520$ MeV), i.e., 0.12 MeV. The cross section due to $N(1520)$ is drastically increased because of the use of the latest value of $\Gamma_{N(1520)\to N\eta}(m = 1520$ MeV), i.e., 0.265 MeV. Due to this, an additional peak appears in the shape of the coherently added cross section. At higher beam energy, i.e., 2.5 GeV, the peak cross section because of $N(1520)$, even for $\Gamma_{N(1520)\to N\eta}(m = 1520$ MeV) $= 0.12$ MeV, supersedes that due to $N(1535)$. The shift of $N(1520)$-peak towards the higher η meson energy (which corresponds to larger resonance mass) depends on the beam energy. This occurs because of the sharp increase in $N(1520) \to N\eta$ decay probability with the resonance mass. The cross section due to $N(1520)$ is further increased by a factor $\sim$5 because of the increase in $\Gamma_{N(1520)\to N\eta}(m = 1520$ MeV) from 0.12 MeV to 0.265 MeV. The coherently added cross section shows that the contribution from $N(1520)$ is distinctly dominant amongst the resonances and Born terms at higher energy. These features are unlike those reported in the previous studies where $N(1535)$ is shown to contribute dominantly in the η meson production reaction.

Acknowledgement

The author gratefully acknowledges the referee for giving valuable comments on this work.

References

[1] J. Beringer, et al., Particle Data Group, Phys. Rev. D 86 (2012) 010001.
[2] E. Oset, H. Toki, W. Weise, Phys. Rep. 83 (1982) 281.
[3] T. Ericson, W. Weise, Pions and Nuclei, Clarendon Press, Oxford, 1988, pp. 242, 325.
[4] D. Drechsel, L. Tiator, S.S. Kamalov, S.N. Yang, Nucl. Phys. A 660 (1999) 423;
E. Oset, W. Weise, Nucl. Phys. A 368 (1981) 375;
M.J.M. van Sambeek, et al., Nucl. Phys. A 631 (1998) 545c.
[5] Q. Ingram, et al., Phys. Lett. B 76 (1978) 173;
E. Oset, W. Weise, Nucl. Phys. A 319 (1979) 477.
[6] J. Chiba, et al., Phys. Rev. Lett. 67 (1991) 1982.
[7] T. Hennino, et al., Phys. Lett. B 283 (1992) 42;
T. Hennino, et al., Phys. Lett. B 303 (1993) 236.
[8] D. Cóntardo, et al., Phys. Lett. B 168 (1986) 331.
[9] Swapan Das, Phys. Rev. C 66 (2002) 014604.
[10] B. Korfgen, F. Osterfeld, T. Udagawa, Phys. Rev. C 50 (1994) 1637.
[11] P.F. de Cordoba, J. Nieves, E. Oset, M.J. Vicente-Vacas, Phys. Lett. B 319 (1993) 416.
[12] B. Lopez Alvaredo, E. Oset, Phys. Lett. B 324 (1994) 125.
[13] W. Peters, H. Lenske, U. Mosel, Nucl. Phys. A 642 (1998) 506.
[14] B.V. Krippa, J.T. Londergan, Phys. Lett. B 286 (1992) 216;
B. Krippa, W. Cassing, U. Mosel, Phys. Lett. B 351 (1995) 406;
J. Lehr, M. Post, U. Mosel, Phys. Rev. C 68 (2003) 044601.
[15] M. Hedayati-Poor, H.S. Sherif, Phys. Rev. C 56 (1997) 1557;
F.X. Lee, L.E. Wright, C. Bennhold, L. Tiator, Nucl. Phys. A 603 (1996) 345.
[16] I.R. Blokland, H.S. Sherif, Nucl. Phys. A 694 (2001) 337.
[17] A. Fix, H. Arenhövel, Nucl. Phys. A 620 (1997) 457;
M. Benmerrouche, N.C. Mukhopadhyay, J.F. Zhang, Phys. Rev. D 51 (1995) 3237.
[18] D.M. Manley, R.A. Arndt, Y. Goradia, V.L. Teplitz, Phys. Rev. D 30 (1984) 904;
D.M. Manley, Phys. Rev. D 51 (1995) 4837;
D.M. Manley, Int. J. Mod. Phys. A 18 (2003) 441.
[19] Swapan Das, Phys. Rev. C 70 (2004) 034604.
[20] H.C. Chiang, E. Oset, L.C. Liu, Phys. Rev. C 44 (1991) 738;
R. Machleidt, K. Holinde, Ch. Elster, Phys. Rep. 149 (1987) 1.
[21] Swapan Das, Phys. Rev. C 72 (2005) 064619;
R.J. Glauber, in: W.E. Brittin, et al. (Eds.), Lectures in Theoretical Physics, vol. 1, Interscience Publishers, New York, 1959.
[22] D.V. Bugg, et al., Phys. Rev. 146 (1966) 980;
S. Barshay, et al., Phys. Rev. C 11 (1975) 360;
W. Grein, Nucl. Phys. B 131 (1977) 255;
C. Lechanoine-Leluc, F. Lehar, Rev. Mod. Phys. 65 (1993) 47;
http://pdg.lbl.gov/xsect/contents.html.
[23] B.K. Jain, N.G. Kelkar, J.T. Londergan, Phys. Rev. C 47 (1993) 1701.
[24] C.W. De Jager, H. De Vries, C. De Vries, At. Data Nucl. Data Tables 14 (1974) 479.